Acta Cryst. (1980). A**36**, 304–315

The Atomic-String Approximation in Cross-Grating High-Energy Electron Diffraction. I. Dispersion Surface and Bloch Waves

BY B. F. BUXTON

Cavendish Laboratory, Madingley Road, Cambridge, CB3 0HE, England

AND P. T. TREMEWAN

H. H. Wills Physics Laboratory, Royal Fort, Tyndall Avenue, Bristol, BS8 1TL, England

(*Received* 13 *September* 1979; *accepted* 22 *October* 1979)

Abstract

A new real-space method of calculating the dispersion surface and Bloch waves in cross-grating HEED is derived. Instead of using a large many-beam matrix to compute the dispersion surface, the equivalent two-dimensional band structure of allowed transverse energies of the Bloch waves is calculated from a small matrix obtained by approximating the KKR equations derived earlier [Ozorio de Almeida (1975). *Acta Cryst.* A**31**, 435–442]. For a close-packed array of atomic strings as in Au [111], transverse energy bands in excellent agreement with conventional 91 × 91 many-beam matrix calculations are obtained with only a 7 × 7 matrix. It is also shown how the calculation of the Bloch waves and their Fourier coefficients $C_{\mathbf{G}}^{(j)}$ may be further simplified by replacing the unit cell of the projected potential by its Wigner–Seitz circle. Numerical calculations, again for Au[111], show that the $C_0^{(j)}$ so obtained are still in excellent agreement with many-beam calculations but that the higher Fourier coefficients $C_{\mathbf{G}}^{(j)}$, being more sensitive to the form of the Bloch waves in the interstitial region, are less accurate. The form of the Bloch waves is investigated and it is shown that near the zone-axis critical voltage, the nearly degenerate Bloch waves are almost entirely *sp* hybrids so that a 3 × 3 matrix may be used.

Introduction

There have been several attempts to extract quantitative information from electron-diffraction zone-axis patterns and channelling patterns (Fujimoto, Takagi, Komaki, Koike & Uchida, 1972; Kambe, Lehmpfuhl & Fujimoto, 1974; Steeds, Jones, Rackham & Shannon, 1976; Shannon & Steeds, 1977). Although useful information about the strength of the string potential has been obtained (Steeds, Jones, Loveluck & Cooke, 1977; Fujimoto, Uchida & Lehmpfuhl, 1976), progress has been hampered by the difficulty of performing the dynamical-diffraction calculations required. In particular, if the dispersion surface and Bloch functions are calculated from the many-beam equations (Hirsch, Howie, Nicholson, Pashley & Whelan, 1965), large matrices (at least of order 60 × 60 even for simple atomic-string potentials) have to be diagonalized to obtain accurate results and the way the observed diffraction depends on the atomic string potentials is obscured. Large matrices are required in these cross-grating orientations with the incident electron beam nearly parallel to a low-index zone axis of the crystal because there are many reciprocal-lattice points in the zero Laue zone which are near the Ewald sphere. The Bloch waves excited in the crystal are therefore made up of many plane-wave components and, to a first approximation, we may regard the electrons as scattered by a two-dimensional projection of the crystal potential (Howie, 1966; Berry, 1971; Buxton, 1976).

Alternatively, we may regard the poor convergence of the many-beam equations as due to the presence of tightly bound Bloch waves sharply peaked on the atomic strings (Kambe, 1978). In fact, it has proved fruitful to describe these bound Bloch waves with negative transverse energy [the zero of transverse energy is taken as the maximum of the projected crystal potential as in Berry (1971) and Ozorio de Almeida (1975*a*)] in terms of localized atomic-string orbitals (Kambe, Lehmpfuhl & Fujimoto, 1974; Buxton, Loveluck & Steeds, 1978*a*,*b*; Uchida, Fujimoto, Katerbau & Wilkens, 1978; Fujimoto, 1978). However, the bound Bloch waves are strongly absorbed (Hirsch *et al.*, 1965; Ozorio de Almeida, 1975*a*,*b*) and contribute little to the observed diffraction from thick crystals which is dominated by the anomalously transmitted Bloch waves with small transverse energies (Steeds, Jones, Loveluck & Cooke, 1977; Fujimoto, Sumida & Fujita, 1977). Moreover, Steeds, Jones, Loveluck & Cooke (1977) show that it is the same Bloch waves with small transverse energies near the maxima of the projected potential which are involved in the zone-axis critical-voltage effect – a dynamical

0567-7394/80/020304-12$01.00

diffraction effect used by these authors to infer the strength of the atomic-string potential. A simple theory capable of describing these Bloch waves with small transverse energies is therefore needed.

Kambe & Lehmpfuhl (1974) and Kambe (1978) have attempted a hybrid description using orthogonalized plane waves (OPWs), but this suffers from the disadvantage that the localized atomic-string orbitals are not known *a priori* unlike the core states in conventional band theory (see Ziman, 1971). In this paper, however, the KKR method proposed by Ozorio de Almeida (1975*a*) will be utilized. Unlike the above OPW and APW (augmented plane wave) methods also proposed by Ozorio de Almeida (1975*a*) which both use an overcomplete set of basis functions, the KKR method has the advantage of being fully analytic as pointed out by Ozorio de Almeida (1975*a*). Furthermore, by using an analogue of Andersen's (1975) atomic-sphere approximation (sometimes called the muffin-tin orbital method), developed recently in conventional band theory, in § 2 we obtain an approximation (hereafter called the *atomic-string approximation* or ASA for short) which enables us to simplify the KKR scheme yet calculate accurately the small transverse energies of the important Bloch waves. Remarkably accurate results are also obtained for the transverse energies of the tightly bound Bloch waves even though the ASA is essentially a small transverse energy approximation.

In § 3, this ASA is discussed in detail for a close-packed array of atomic-string potentials and numerical results given for [111] zone axes of Au and Mo. In the ASA, the projected potential is replaced by a muffin-tin potential as described by Ozorio de Almeida (1975*a*) in his derivation of the KKR. For a close-packed array of atomic strings as in Au [111] and Mo [111], it is obviously a good approximation to replace the projected potential $U(\mathbf{R})$ by a muffin-tin potential which is cylindrically symmetric within muffin-tin cylinders of radius R_M about the centre of each atomic string and constant in the interstitial regions as found by Jones (1976) in his APW calculations. However, for the more open arrangements of atomic strings often encountered when there are two or more strings of atoms in each unit cell of the projected potential, as in the [0001] zone axis of $2H_1$ MoS_2 or Si⟨110⟩, the muffin-tin approximation can lead to serious errors (Jones, 1976). In the ASA we also ignore the detailed geometry of the unit cell of the projected potential when calculating the Bloch waves themselves. Nevertheless, as shown in § 4, the ASA still enables us to calculate the Bloch waves fairly accurately, particularly as far as cylindrical averages of them are concerned. Thus, for example, the Fourier coefficients $C_0^{(j)}$ are found to be in excellent agreement with conventional many-beam calculations. Furthermore, with small matrices, often only 3 × 3, we obtain formulae sufficiently simple to enable us to investigate the zone-axis critical-voltage effect analytically in a following paper.

2. Derivation of the ASA from the KKR

2.1 *The muffin-tin potential and the KKR*

As described in several papers (Berry, 1971; Ozorio de Almeida 1975*a*; Buxton, 1976), in the projection approximation we expand the electron wavefunction in the crystalline specimen in terms of the two-dimensional Bloch waves $\tau_j(\mathbf{R})$ which have transverse energies s_j. Thus,

$$\psi(\mathbf{r}) = \exp(i\chi z) \sum_j \varepsilon_j \tau_j(\mathbf{R}) \exp(-i s_j z/2\chi), \quad (2.1)$$

where it is assumed that the zone axis is parallel to the z axis, that $\mathbf{R}$ is the component of $\mathbf{r}$ perpendicular to $\mathbf{z}$ and that the entrance surface of the crystal is the plane $z = 0$ on which (2.1) is matched to an incident plane wave $e^{i\chi \cdot \mathbf{r}}$. If $\mathbf{K}$ is the component of the incident wavevector $\boldsymbol{\chi}$ perpendicular to $\mathbf{z}$, the excitation amplitudes ε_j are given by the initial condition

$$e^{i\mathbf{K}.\mathbf{R}} = \sum_j \varepsilon_j \tau_j(\mathbf{R}) \quad (2.2)$$

since the expansion (2.1) neglects back-scattered waves (Buxton, 1976).

The Bloch waves $\tau_j(\mathbf{R})$ are eigenfunctions of the two-dimensional Schrödinger equation

$$[-\nabla_{\mathbf{R}}^2 + \bar{U}(\mathbf{R})]\, \tau_j(\mathbf{R}) = s_j(\mathbf{K})\, \tau_j(\mathbf{R}), \quad (2.3)$$

with the Bloch boundary condition

$$\tau_j(\mathbf{R} + \mathbf{L}) = e^{i\mathbf{K}.\mathbf{L}} \tau_j(\mathbf{R}), \quad (2.4)$$

in which $\mathbf{L}$ is a lattice vector of the projected potential $\bar{U}(\mathbf{R})$. Our central problem is to calculate these two-dimensional Bloch functions $\tau_j(\mathbf{R})$ and the two-dimensional band structure $s_j(\mathbf{K})$ from which the dispersion surface of allowed wavevectors $\chi - s_j(\mathbf{K})/2\chi$ is easily obtained as explained by Ozorio de Almeida (1975*a*) and Buxton (1976).

In the many-beam theory the projected potential is written in terms of its Fourier coefficients

$$\bar{U}(\mathbf{R}) = \sum_{\mathbf{G}} U_{\mathbf{G}}\, e^{i\mathbf{G}.\mathbf{R}}, \quad (2.5)$$

where the summation is over reciprocal-lattice vectors $\mathbf{G}$ perpendicular to the zone axis $\mathbf{z}$. The Bloch waves are similarly expanded:

$$\tau_j(\mathbf{R}) = \sum_{\mathbf{G}} C_{\mathbf{G}}^{(j)}\, e^{i(\mathbf{K}+\mathbf{G}).\mathbf{R}}. \quad (2.6)$$

Substitution of these expansions in (2.3) yields the familiar many-beam equations:

$$\sum_{\mathbf{G}'} \{[s_j(\mathbf{K}) - (\mathbf{K} + \mathbf{G})^2]\, \delta_{\mathbf{G}\mathbf{G}'} - U_{\mathbf{G}-\mathbf{G}'}\} C_{\mathbf{G}'}^{(j)}(\mathbf{K}) = 0, \tag{2.7}$$

from which the transverse energy band structure, $s_j(\mathbf{K})$, and the Fourier coefficients of the Bloch waves, $C_{\mathbf{G}}^{(j)}$, may be obtained by matrix diagonalization. Since in this paper we shall not attempt to calculate diffracted wave intensities or fine details of the behaviour of the Bloch waves, absorption effects will be neglected. The potential, $\tilde{U}(\mathbf{R})$, and the transverse energies, $s_j(\mathbf{K})$, are therefore real. In any case, absorption effects can often be included afterwards by non-degenerate perturbation theory without affecting the Bloch waves or the real part of the transverse energy although a more careful calculation is necessary near the zone-axis critical voltage (David, Gevers & Serneels, 1976; Buxton & Loveluck, 1977).

In the KKR method, we exploit the approximate cylindrical symmetry of the projected potential within each atomic string and replace $\tilde{U}(\mathbf{R})$ by a muffin-tin potential $U_{MT}(R)$ obtained by taking an angular average about the centre of each atomic string which is assumed to be at $\mathbf{R} = 0$. Thus,

$$U_{MT}(R) = \sum_{\mathbf{G}} U_{\mathbf{G}} J_0(GR) \quad \text{for } R < R_M, \tag{2.8}$$

where R_M is the muffin-tin radius. Since the average interstitial potential is chosen to be zero, the average potential U_0 is given by

$$U_0 = \frac{2\pi R_M^2}{S_0 - \pi R_M^2} \sum_{\mathbf{G}\neq 0} U_{\mathbf{G}} \frac{J_1(GR_M)}{GR_M}, \tag{2.9}$$

in which S_0 is the area of a unit cell of the projected potential and $S_0 - \pi R_M^2$ is the interstitial area. If, as assumed here, there is only one atomic string in each unit cell of the projected potential, the best approximation with the smallest interstitial area is obtained by allowing the muffin-tin cylinders to touch, so that R_M is half the string spacing.

Inside each muffin-tin cylinder, we now expand the Bloch functions $\tau_j(\mathbf{R})$ in a partial wave series using the cylindrical harmonics $e^{il\theta}$ and the regular solutions $\tau_l(\mathbf{R})$ of the radial Schrödinger equation (Berry & Ozorio de Almeida, 1973):

$$-\frac{1}{R}\frac{\mathrm{d}}{\mathrm{d}R} R \frac{\mathrm{d}\tau_l}{\mathrm{d}R} + [U_{MT}(R) + l^2/R^2]\, \tau_l = \kappa^2 \tau_l, \tag{2.10}$$

in which κ^2 is equal to s the transverse energy. Thus, for $R < R_M$,

$$\tau_j(\mathbf{R}) = \sum_{l=-\infty}^{\infty} a_l^{(j)} e^{il\theta} \tau_l(R), \tag{2.11}$$

the coefficients $a_l^{(j)}$ being obtained from the eigenvectors of the KKR equations (Ozorio de Almeida, 1975*a*)

$$\sum_{l'} [(\cot \eta_l - i)\, \delta_{ll'} + \mathscr{G}'_{ll'}] \sin(\eta_{l'})\, a_{l'} = 0. \tag{2.12}$$

These equations also determine the transverse energy, s, since there are only non-trivial eigenvectors at particular energies, s_j, when the waves scattered by all the atomic strings interfere constructively to form Bloch functions.

In (2.12), the scattering properties of the individual muffin-tin potentials enter through the phase shifts η_l which may be obtained from numerical solutions of the Schrödinger equation (2.10) *via* the log derivatives

$$D_l(s) = [R\tau_l'(R)/\tau_l(R)]_{R=R_M}, \tag{2.13}$$

since

$$\cot \eta_l(s) = (R_M Y_l' - D_l Y_l)/(R_M J_l' - D_l J_l). \tag{2.14}$$

Here, all the Bessel functions are evaluated at κR_M and the $'$ denotes differentiation with respect to R.

The structure constants, $\mathscr{G}'_{ll'}(s,\mathbf{K})$, however, only depend on the geometrical arrangement of the atomic strings (Ozorio de Almeida, 1975*a*). Since we are seeking stationary-state eigenfunctions $\tau_j(\mathbf{R})$, the $\mathscr{G}'_{ll'}$ must be obtained from the principal value Green's function so, for negative s,

$$\mathscr{G}'_{ll'} = -i \sum_{\mathbf{L}\neq 0} e^{i\mathbf{K}.\mathbf{L}} H^{(1)}_{l-l'}(\kappa L)\, e^{il\theta_{\mathbf{L}}}, \tag{2.15}$$

where $\kappa = i\sqrt{-s}$. For positive s, the Hankel function $H^{(1)}_{l-l'}$ must be replaced by i times a Neumann function $Y_{l-l'}$ and the $-i$ after the cot η_l in (2.12) omitted so that the KKR matrix is always Hermitian when, as here, absorption is neglected. Although the lattice sum in (2.15) for $s < 0$ is rapidly convergent, when s is positive the corresponding series must be summed by an Ewald transformation (Ozorio de Almeida, 1975*a*).

2.2 *The atomic-string approximation*

The ASA is obtained from (2.12) in two steps. First, we let $\kappa \to 0$ everywhere *except* in the log derivatives $D_l(s)$ where we retain the transverse energy, s, and *then* we replace the muffin-tin cylinder by the slightly larger Wigner–Seitz cylinder of radius R_s chosen such that πR_s^2 is equal to the area of a unit cell S_0. Physically, this is because we expect the transverse energy bands, $s_j(\mathbf{K})$, to be relatively insensitive to the value assigned to the flat interstitial potential, so for small s we may take the interstitial potential to be equal to the transverse energy which implies $\kappa = 0$ in the interstitial region. We then replace R_M by R_s to mimimize the interstitial area in which the Bloch waves have been approximated (Andersen, 1975).

Since (Abramowitz & Stegun, 1965), for positive n as $x \to 0$,

$$H_n^{(1)}(x) \simeq iY_n(x) \simeq -i\frac{(n-1)!}{\pi}\left(\frac{2}{x}\right)^n$$

and (2.16)

$$H_0^{(1)}(x) \simeq iY_0(x) \simeq \frac{2i}{\pi}\ln(x),$$

the same limiting formulae are obtained in (2.12) when $\kappa \to 0$ along the positive real axis or the positive imaginary axis. Using (2.14), the fact that

$$J_n(x) \underset{x\to 0}{\simeq} \frac{1}{n!}\left(\frac{x}{2}\right)^n \quad \text{for } n \geq 0, \tag{2.17}$$

and the relation

$$\mathscr{C}_{-n}(x) = (-1)^n \mathscr{C}_n(x), \tag{2.18}$$

which holds for all cylinder functions, we find for example that

$$\mathscr{G}'_{ll'} \to -\sum_{\mathbf{L}\neq 0} e^{i\mathbf{K}.\mathbf{L}}[(|l-l'|-1)!/\pi] \times (2\sigma_{l-l'}/\kappa L)^{|l-l'|}\exp[-i(l-l')\,\theta_{\mathbf{L}}] \tag{2.19}$$

for $l \neq l'$, where $\sigma_{l-l'}$ is ± 1 according as $l \gtrless l'$. Similarly, for $l \neq 0$,

$$\cot \eta_l \to \left(\frac{2}{\kappa R_M}\right)^{2|l|} \frac{|l|!(|l|-1)!}{\pi}\frac{|l|+D_l}{|l|-D_l} \tag{2.20}$$

as $\kappa \to 0$. Since, according to (2.16), $\mathscr{G}'_{ll}$ only diverges as $\ln(\kappa)$, the phase-shift terms (2.20) are much larger than the diagonal structure constants $\mathscr{G}'_{ll}$. However, the s wave phase shift

$$\cot \eta_0 \to \frac{-2}{\pi D_0} + \frac{2}{\pi}[\ln(\kappa R_M/2) + \gamma] \tag{2.21}$$

and only diverges as fast as the structure constant $\mathscr{G}'_{00}$ (γ is Euler's constant equal to 0·5772). A careful calculation using

$$\sum_{\mathbf{L}\neq 0} e^{i\mathbf{K}.\mathbf{L}} = -1 \quad \text{when } \mathbf{K} \neq \mathbf{G} \tag{2.22}$$

then shows that the logarithmically divergent terms in $\cot \eta_0$ and $\mathscr{G}'_{00}$ cancel, and that

$$\cot \eta_0 - i + \mathscr{G}'_{00} \to \frac{-2}{\pi D_0} + \frac{2}{\pi}\sum_{\mathbf{L}\neq 0} e^{i\mathbf{K}.\mathbf{L}}\ln(L/R_M). \tag{2.23}$$

Thus, as we let $\kappa \to 0$, the diagonal terms in the KKR matrix diverge as $\kappa^{-2|l|}$ and the off-diagonal terms as $\kappa^{-|l-l'|}$. Part of this divergence is cancelled by the $\sin \eta_{l'}$ terms in (2.12), for which as $\kappa \to 0$

$$\sin \eta_{l'} \to \frac{\pi}{2}\left(\frac{\sigma_{l'}\kappa R_M}{2}\right)^{|l'|}\frac{1}{|l'|!}\tau_{l'}(R_M)\,[|l'| - D_{l'}] \tag{2.24}$$

but the remainder has to be removed by multiplying each equation in (2.12) by $(\sigma_l \kappa R_M/2)\,\pi/(2|l|!)$. If we then replace R_M by the Wigner–Seitz radius R_s, we obtain the ASA equations:

$$\sum_{l'}\{f_l[D_l(s,R_s)]\,\delta_{ll'} + \mathscr{S}_{ll'}(\mathbf{K})\}\,c_{l'} = 0, \tag{2.25}$$

in which the log derivatives D_l are now evaluated at R_s and appear only on the diagonal in the combinations:

$$f_l(D_l) = \begin{cases} \dfrac{1}{2|l|}\dfrac{|l|+D_l}{|l|-D_l} & \text{for } l \neq 0 \\ -1/D_0 & \text{for } l = 0. \end{cases} \tag{2.26}$$

The new structure constants $\mathscr{S}_{ll'}(\mathbf{K})$ are independent of the transverse energy and can be evaluated once and for all at the beginning of a calculation. Because the original KKR structure constants $\mathscr{G}'_{ll'}$ only diverged as $\kappa^{-|l-l'|}$ and each off-diagonal term has effectively been multiplied by $\kappa^{|l|+|l'|}$ as we took the small κ limit, the ASA structure constants, $\mathscr{S}_{ll'}$, vanish if l and l' are non-zero and have the same sign. The remaining structure constants, however, cannot be computed from the series given in (2.19) and (2.23) because they do not converge very quickly. An Ewald transformation must therefore be used as described by Nijboer & de Wette (1957). Alternatively, we can take the small κ limit of the formulae given by Ozorio de Almeida (1975*a*). Thus, for $ll' \leq 0$ and $l \neq l'$,

$$\mathscr{S}_{ll'}(\mathbf{K}) = \frac{-(-1)^{|l'|}}{|l|!|l'|!}\left[\frac{2\pi}{S_0}\,i^{|l|+|l'|} \times \sum_{\mathbf{G}}\frac{e^{-(\mathbf{K}+\mathbf{G})^2 X}}{(\mathbf{K}+\mathbf{G})^2}\,e^{-i(l-l')\theta_{\mathbf{K}+\mathbf{G}}} \times (R_s|\mathbf{K}+\mathbf{G}|/2)^{|l-l'|} + \tfrac{1}{2}\sum_{\mathbf{L}\neq 0} e^{i\mathbf{K}.\mathbf{L}}e^{-i(l-l')\theta_{\mathbf{L}}} \times (R_s L/4X)^{|l-l'|}\alpha_{|l-l'|-1}(L^2/4X)\right] \tag{2.27}$$

and

$$\mathscr{S}_{00}(\mathbf{K}) = \frac{-2\pi}{S_0}\sum_{\mathbf{G}}\frac{e^{-(\mathbf{K}+\mathbf{G})^2 X}}{(\mathbf{K}+\mathbf{G})^2} - \tfrac{1}{2}\sum_{\mathbf{L}\neq 0} e^{i\mathbf{K}.\mathbf{L}}E_1(L^2/4X) + \tfrac{1}{2}[\gamma - \ln(4X/R_s^2)], \tag{2.28}$$

where the exponential integrals α_n and E_1 are defined as in Abramowitz & Stegun (1965). The Ewald parameter

X may conveniently be taken as $S_0/4\pi$, which for a square or hexagonal lattice secures equally rapid convergence of the direct and reciprocal-lattice sums. Note that, apart from trivial factors and complex conjugation, the structure constants depend only on $|l-l'|$.

Finally, we note that on a transverse energy band, $s_j(\mathbf{K})$, when the secular determinant

$$\det_{ll'}|f_l[D_l(s_j)]\,\delta_{ll'}+\mathscr{S}_{ll'}(\mathbf{K})|=0, \qquad (2.29)$$

the partial wave amplitudes, $a_l^{(j)}$, in (2.11) may be obtained from the ASA eigenvectors, since

$$c_l^{(j)}=\frac{\tau_l(R_s)}{R_s}\,[|l|-D_l]\,a_l^{(j)}. \qquad (2.30)$$

3. The ASA for hexagonal close-packed atomic strings

Shannon & Steeds (1977) have discussed the qualitative features of high-symmetry zone-axis patterns obtained from several different arrangements of atomic-string potentials. The simplest is the hexagonal close-packed array obtained, for example, from a $\langle 111\rangle$ zone axis of a f.c.c. or b.c.c. metal which will be discussed here in detail. A similar analysis may be carried out for other simple (*e.g.* square or rectangular) arrays. The form of the dispersion surface is determined by the behaviour of the structure constants $\mathscr{S}_{ll'}(\mathbf{K})$ and the form of the log derivatives $D_l(s)$. As in the KKR, the structure constants depend only on the geometrical arrangement of the atomic strings, whilst the log derivatives depend only on the form of the muffin-tin potential $U_{MT}(R)$.

3.1 *The ASA structure constants* $\mathscr{S}_{ll'}(\mathbf{K})$

To obtain a good impression of the form of the dispersion surface for the *6mm* zone axes of interest here, we may plot the transverse energy bands, $s_j(\mathbf{K})$, along the symmetry lines in the two-dimensional Brillouin zone as indicated in Shannon & Steeds (1977) and in Fig. 1. Computed values of the non-zero *ss*, *sp* and *pp* structure constants obtained from (2.27) and (2.28) along $\bar{\Sigma}$ and $\bar{T}$ are shown in Fig. 2. Since the ASA structure constants are independent of the size of the hexagonal lattice $\{\mathbf{L}\}$, for convenience a [111] zone axis of a f.c.c. crystal with its lattice parameter set equal to unity has been assumed. Usually, with the Ewald parameter X chosen as described in § 2, only three or four stars of vectors were required in each sum to obtain the structure constants to an accuracy of 10^{-5}.

In Fig. 2, the structure constants have been multiplied by $K^{2-|l|-|l'|}$ to cancel the divergence of the $\mathbf{G}=0$ term at the $\bar{\Gamma}$ point and also by factors of i and $e^{i(l-l')\theta_K}$ to obtain a real positive result. Also shown in

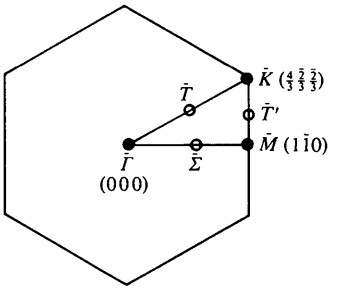

Fig. 1. Symmetry lines in the two-dimensional Brillouin zone for a *6mm* zone axis. The Miller indices correspond to a [111] zone axis of a f.c.c. crystal.

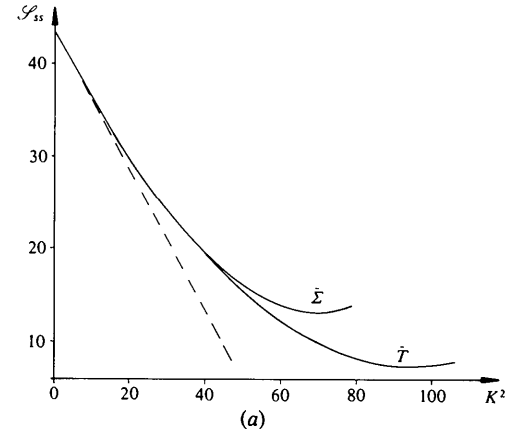

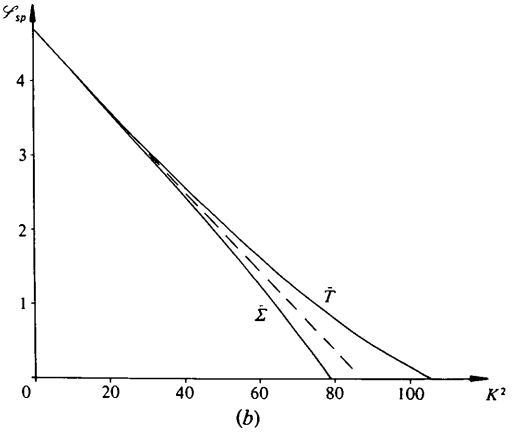

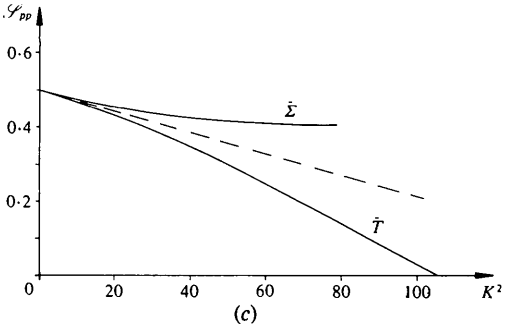

Fig. 2. ASA structure constants as functions of K^2 along $\bar{\Sigma}$ and $\bar{T}$.

Fig. 2 as a dashed line is an analytic approximation obtained by expanding (2.27) about $K = 0$ and using symmetry and the Poisson summation formula (Lighthill, 1958) to eliminate the sums for the *sp* and *pp* structure constants. In detail, for our hexagonal array we find:

$$\begin{aligned} \mathscr{S}_{00} &\simeq -2(KR_s)^{-2} + 0{\cdot}7488 \\ \mathscr{S}_{0-1} &\simeq i[(KR_s)^{-1} - KR_s/4]\, e^{-i\theta_K} \\ \mathscr{S}_{1-1} &\simeq -\tfrac{1}{2}[1 - (KR_s)^2/8]\, e^{-2i\theta_K}, \end{aligned} \tag{3.1}$$

where 0·7488 is the value of the constant term in $\mathscr{S}_{00}$ obtained by summing series similar to those in (2.28) if we set $\mathbf{K} = 0$ and omit the $\mathbf{G} = 0$ term. Unlike the *pp* structure constant which tends to a constant at $\bar{\Gamma}$, the higher structure constants vanish as $\mathbf{K} \to 0$ unless $|l - l'|$ is a multiple of six, in which case the sums over the non-zero $\mathbf{L}$ and $\mathbf{G}$ in (2.27) no longer vanish due to the symmetry, but tend to a constant value.

Similarly, we may use the *2mm* symmetry about the $\bar{M}$ point and the *3m* symmetry at $\bar{K}$ to show that the structure constants vanish unless $|l - l'|$ is a multiple of two or three respectively. Thus, $\mathscr{S}_{0-1}$ vanishes at both $\bar{M}$ and $\bar{K}$ as in Fig. 2(*b*), but $\mathscr{S}_{1-1}$ only vanishes at $\bar{K}$. Technically, these properties are due to the fact that the point group of $\mathbf{K}$ is *6mm*, *2mm* and *3m* at $\bar{\Gamma}$, $\bar{M}$ and $\bar{K}$ respectively (Buxton, Loveluck & Steeds, 1978*b*; Cornwell, 1969).

We may now deduce quite a lot about the coupling of the various partial waves in (2.11). For example, at $\bar{K}$ a 3 × 3 *sp* secular determinant (2.29) is diagonal giving pure *s* and *p* wave solutions at which

$$\begin{aligned} D_0 &= 1/\mathscr{S}_{00} = -13{\cdot}296 \ (s \text{ wave}) \\ \text{and} \qquad D_1 &= -1 \ (p \text{ wave doublet}). \end{aligned} \tag{3.2}$$

The *p* wave solution is a doublet as demanded by group theory – there is a two-dimensional irreducible representation of the point group of $\mathbf{K}$ at $\bar{K}$ (Buxton, Loveluck & Steeds, 1978*b*; Bradley & Cracknell, 1972). Furthermore, since the structure constants $\mathscr{S}_{ll'}$ vanish at $\bar{K}$ unless $|l - l'|$ is a multiple of three, the *s* state can only couple to $f(|l| = 3)$ or higher partial waves with $l = 3n$ as the size of the ASA determinant is increased. The *p* states on the other hand couple to *d*, *g*, *etc.*, since *l* and *l'* can be negative as well as positive. In either case, the strength of the coupling is determined by the scattering properties of the potential *via* the log derivatives $D_l(s)$. Similarly, at $\bar{M}$ even partial waves (*s*, *d*, *g*, ...) are coupled as are the odd ones. Again these conclusions have been confirmed by a group-theoretical analysis using projection operator techniques as described by Bradley & Cracknell (1972).

However, at $\bar{\Gamma}$ the situation is more complicated. From group theory, Buxton, Loveluck & Steeds (1978*b*) have deduced that $|l|$ and $|l'| = 0$ and 6, 1 and 5, 2 and 4, *etc.* are coupled in accordance with the rule that $|l - l'|$ should be a multiple of six which is just the condition that the structure constants involving *f* or higher angular momenta do *not* vanish as $\mathbf{K} \to 0$. The problem is that in the 3 × 3 determinant,

$$\begin{vmatrix} \frac{1}{2}\frac{1+D_1}{1-D_1} & \mathscr{S}_{-10} & \mathscr{S}_{-11} \\ \mathscr{S}_{0-1} & -\frac{1}{D_0} + \mathscr{S}_{00} & \mathscr{S}_{01} \\ \mathscr{S}_{1-1} & \mathscr{S}_{10} & \frac{1}{2}\frac{1+D_1}{1-D_1} \end{vmatrix} = 0, \tag{3.3}$$

the *s* and *p* waves are apparently coupled. However, if we take the leading terms in (3.1) for the structure constants and retain $1/D_0$ as a term also of order K^{-2}, we find on expanding (3.3) that

$$\begin{aligned} [D_0 + (KR_s)^2/2]\left(\frac{1+D_1}{1-D_1}\right)^2 + 2D_0\left(\frac{1+D_1}{1-D_1}\right) \\ + [D_0 - (KR_s)^2/2] = 0, \end{aligned} \tag{3.4}$$

which has solutions

$$D_0 = 0 \quad \text{and} \quad 1/D_1 = 0 \text{ (twice)} \tag{3.5}$$

as $\mathbf{K} \to 0$; *i.e.* the *s* and *p* waves are not really coupled. Of course, we do not know *a priori* that $1/D_0$ will diverge at one of the roots and should be regarded as $O(K^{-2})$. However, if we expand (3.3) including terms of order K^{-2} and K^0 using the approximations given in (3.1), we find the same solutions (3.5). Moreover, by continuing to regard $1/D_0$ as $O(K^{-2})$ as above, it can be shown by picking out the terms of order K^{-2} in larger determinants that partial waves *l* and *l'* are only coupled at $\bar{\Gamma}$ if $|l - l'|$ is divisible by six as demanded by group theory. It should also be noted that *p* and *d* wave solutions retain their twofold degeneracy (Buxton, Loveluck & Steeds, 1978*b*).

3.2 *The log derivatives* $D_l(s)$

As noted previously, the form of the muffin-tin potential only affects the form of the log derivatives $D_l(s)$ which may be obtained by numerical integration of the radial Schrödinger equation (2.10) outward from the origin. This presents no problems since thermal vibrations smear out the Coulomb singularity in the potential at the centre of the atomic string so that $U_{MT}(R)$ has a smooth parabolic minimum at $R = 0$ (Ozorio de Almeida, 1975*a*; Buxton, Loveluck & Steeds, 1978*b*) and we may begin the integration with

$$\tau_l(R) = J_l\{R[s - U_{MT}(0)]^{1/2}\} \tag{3.6}$$

for very small *R* (Jones, 1977). Since the projected potential $\bar{U}(\mathbf{R})$ is proportional to the relativistic mass of the fast electrons (Fujiwara, 1961, 1962), the integration is repeated for each incident beam energy of interest. Fig. 3 shows the log derivatives for a Au [111]

zone axis at room temperature for 613 keV incident electrons. Just as in the more familiar one- or three-dimensional cases, the log derivatives are monotonic decreasing functions of the (transverse) energy, s, with simple poles whenever a zero of $\tau_l(R)$ crosses the Wigner–Seitz radius as s is increased (Messiah, 1961).

In the example shown in Fig. 3, there is a tightly bound 1s state of the potential $U_{MT}(R)$ very near the sharp pole in D_0 at $s \simeq -47$ Å^{-2} since, according to Ozorio de Almeida (1975*b*),

$$D_l(s) = |\kappa| R_s K_l'(|\kappa| R_s)/K_l(|\kappa| R_s), \\ \rightarrow |\kappa| R_s \quad \text{as } s \rightarrow -\infty \tag{3.7}$$

at a deeply-bound state. However, when an outer node of $\tau_l(R)$ moves in across R_s as s increases through positive values, the pole in D_l is much broader as in D_0 near $s = 15$ Å^{-2} in Fig. 3.

3.3 *The form of the dispersion surface and convergence of the ASA*

Once the structure constants and the log derivatives have been calculated as outlined in the preceding sections, we may calculate the transverse energy bands, $s_j(\mathbf{K})$, and hence the dispersion surface by finding the zeros of the ASA determinant (2.29). For the hexagonal zone axis of interest here, a 7 × 7 determinant including only s, p, d and f partial waves proved sufficient for an accurate calculation of the important energy bands with $s_j(\mathbf{K})$ small or negative. The roots, $s_j(\mathbf{K})$, of this highly non-linear secular determinant were found by the method described in the Appendix, which essentially involves the construction of a Sturm sequence followed by binary chopping to locate the roots. For Au [111] at 293 K and 613 keV the results are shown in Fig. 4 together with many-beam eigenvalues computed from (2.7). As can be seen, near $\bar{\Gamma}$ a 3 × 3 determinant including only s and p waves may be used.

We can see this in detail by considering the way the partial waves are coupled. At $\bar{\Gamma}$ an s wave can only be coupled to other waves with $l = 6n$, but states of such large angular momentum occur only at very high transverse energies so hybridization with the low-lying s states is negligible. Similarly, the low-lying p states are scarcely hybridized with the high $g(|l| = 4)$ states. At $\bar{K}$ however, it is essential to include the f waves because the high s state on the fourth band near $s_4 = 10$ Å^{-2} is forced down by hybridization with the higher f states. The low-lying p states on bands (2) and (3) near $s = -2$ are again little affected by hybridization with higher d states. In contrast, at $\bar{M}$ where only even or odd partial waves can be coupled, the inclusion of the f waves does not affect the highest s state which is strongly hybridized with the d waves, moving down from around 9 to 6 Å^{-2} when a 5 × 5 matrix is used instead of a 3 × 3.

Thus, in the region just above and below $s = 0$ which includes the states contributing most to the observed diffraction from thick Au [111] crystals at this voltage, there are three hybridized bands of predominantly sp character. At higher voltages, these bands become tightly bound with negative s as described by Buxton, Loveluck & Steeds (1978*a*,*b*). Indeed, at 1 MeV, the 2p bands are already quite narrow as shown in Fig. 5(*a*).

To understand how the ASA which is a small transverse energy approximation enables us to calculate the position of these bound bands and even the very deeply bound 1s band, we have only to recall the form of the log derivatives D_l near a deeply bound state as described in § 3.2. Thus, for example, although the ASA condition for the 1s state varies around the

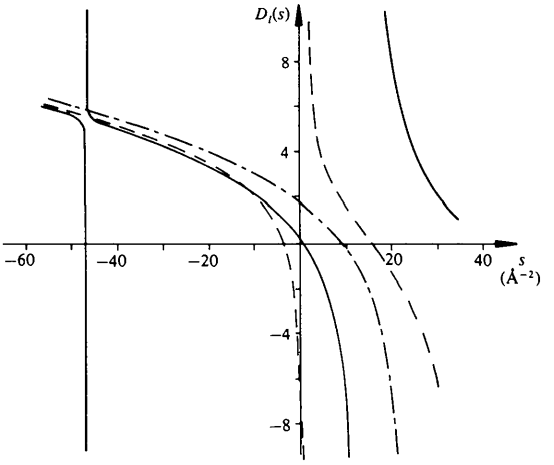

Fig. 3. s(——), p(– – –) and d(–·–·–) log derivatives for Au [111].

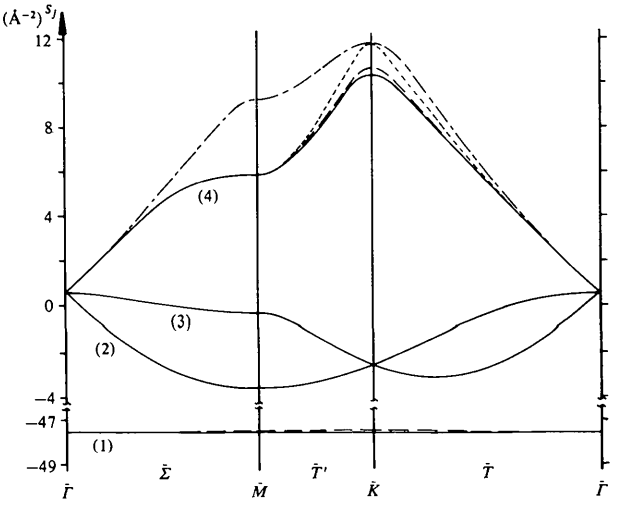

Fig. 4. The first four transverse energy bands for Au [111] at 613 keV from the ASA with a 3 × 3 (–·–·–·–), 5 × 5(·····) and 7 × 7 (——) matrix. The (– – –) lines are the results of a many-beam calculation using a 91 × 91 matrix along $\bar{T}$ and $\bar{\Sigma}$ and an 80 × 80 matrix along $\bar{T}'$.

Brillouin zone according to

$$1/D_0 = \mathscr{S}_{00}(\mathbf{K}), \tag{3.8}$$

which implies

$$D_0 = \begin{cases} 0 & \text{at } \bar{\Gamma} \\ -13{\cdot}296 & \text{at } \bar{K} \\ -5{\cdot}701 & \text{at } \bar{M} \end{cases}; \tag{3.9}$$

near the 1s bound state given by (3.7) D_0 varies so rapidly that all these values are attained at almost the same transverse energy.

In Fig. 5(b), results are given for Au [111] at 100 keV when bands (2), (3) and (4) lie considerably above $s = 0$. The ASA still gives accurate results although it must break down eventually for very high free bands when $s \gg |U_0|$. We note especially that bands (2), (3) and (4) which become accidentally degenerate at 613 keV (Fig. 4) are accurately described in the ASA throughout the range 100 to 1000 keV. Thus, we conclude that the singlet Γ_1 and doublet Γ_5 states which become degenerate at the zone-axis critical voltage of 613 keV, as above (Shannon & Steeds, 1977; Steeds, Jones, Loveluck & Cooke, 1977; Buxton & Tremewan, 1978), are s and p states respectively, just as at very high voltage when they correspond to 2s and 2p atomic-string bound states (Buxton, Loveluck & Steeds, 1978a,b).

Similarly, the ASA may be used to calculate the transverse energy bands near higher zone-axis critical voltages such as that involving bands (7) (8) and (9) in Mo [111] (Steeds, Jones, Loveluck & Cooke, 1977). Fig. 6(a) shows results computed at 830 keV, the predicted value of this critical voltage from a 91 × 91 many-beam calculation. There is now quite a large dis-

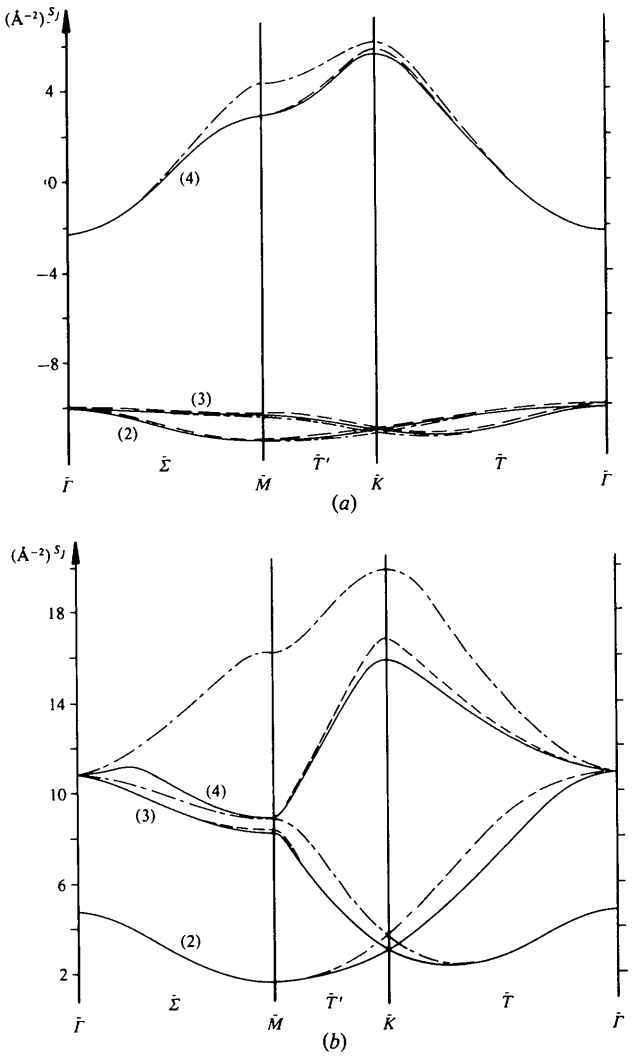

Fig. 5. Bands (2), (3) and (4) for Au [111] at 293 K for (a) 1 MeV, (b) 100 keV incident electrons from a 3 × 3 (–·–·–·) and 7 × 7 (——) ASA matrix compared with many-beam results computed as in Fig. 4.

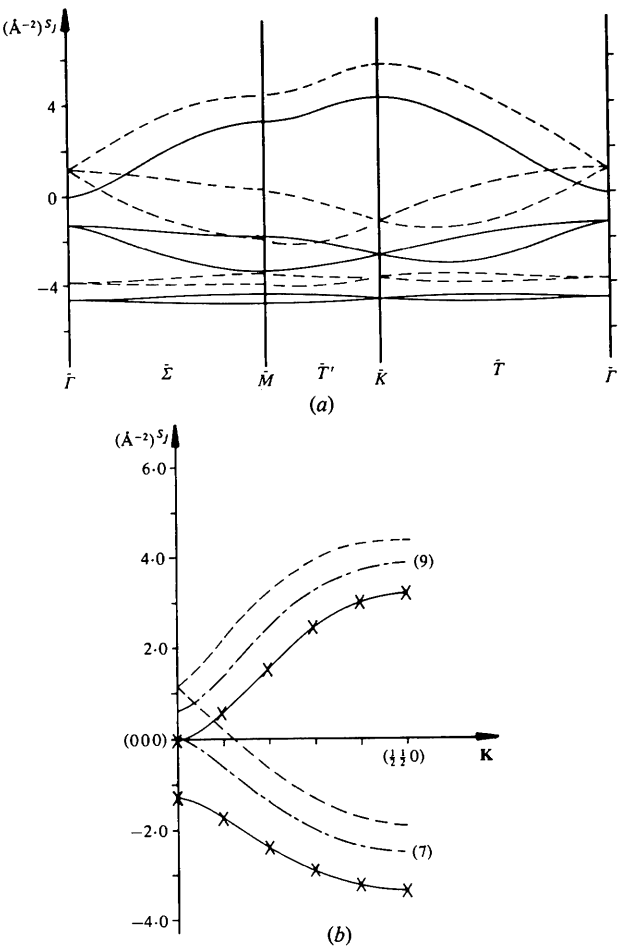

Fig. 6. Mo [111], (a) bands (5)–(9) (——) from a 7 × 7 ASA matrix and (– – –) from a many-beam matrix computed again as in Fig. 4. (b) Comparison of ASA (——) and 91 × 91 (– – –) and 127 × 127 (–·–·–·) many-beam calculations. The convergence of the ASA is confirmed by the APW results × calculated as in Jones (1976).

crepancy between the ASA and many-beam results, but as Fig. 6(*b*) shows, this is due to lack of convergence of the many-beam calculation for this very deep, strong potential.

4. Bloch waves in the ASA

As noted at the end of § 2.2, the partial wave amplitudes, $a_l^{(j)}$, may be obtained from the eigenvectors, $\{c_l^{(j)}\}$, of the ASA equations, (2.25). The latter are best obtained by inverse iteration (Wilkinson, 1965) using the (approximately) singular ASA matrix evaluated at the transverse energy $s_j(\mathbf{K})$. For this, any essential degeneracies of the $s_j(\mathbf{K})$ must be split by evaluating the matrix at a neighbouring $\mathbf{K}$ point of lower symmetry. Once we have found the $c_l^{(j)}$, the partial wave amplitudes, $a_l^{(j)}$, given by

$$a_l^{(j)} = R_s\, c_l^{(j)} / [\tau_l(R_s)(|l| - D_l)] \tag{4.1}$$

must be normalized. It is usual to choose

$$1/S_0 \int_{S_0} \mathrm{d}^2\,\mathbf{R}\,|\tau_j(\mathbf{R})|^2 = 1, \tag{4.2}$$

so that for the Fourier coefficients,

$$\sum_{\mathbf{G}} |C_{\mathbf{G}}^{(j)}|^2 = 1. \tag{4.3}$$

In the full KKR method this is quite difficult because (4.2) involves integration over the muffin-tin cylinder and the interstitial area (Ozorio de Almeida, 1975*a*). However, in the ASA where it has been assumed that the partial wave expansion (2.11) is valid out to the Wigner–Seitz radius R_s, we may replace the integral over the complicated geometry of the unit cell S_0 by an integral over the Wigner–Seitz circle. Thus, performing the angular integration, we demand

$$\sum_l \left|a_l^{(j)}\right|^2 2\pi/S_0 \int_0^{R_s} R\,\mathrm{d}R\,\tau_l^2(R) = 1, \tag{4.4}$$

in which the radial integration may be evaluated by means of the Wronskian theorem (Messiah, 1961);

$$\int_0^{R_s} R\,\mathrm{d}R\,\tau_l^2 = R_s\left[\tau_l' \frac{\partial \tau_l}{\partial s} - \tau_l \frac{\delta \tau_{l'}}{\delta s}\right]_{R_s} \tag{4.5}$$

$$= -\,\tau_l^2(R_s)\frac{\partial D_l}{\partial s}.$$

Similarly, once we have normalized the amplitudes $a_l^{(j)}$, it is easy to calculate the Fourier coefficients of the Bloch waves since

$$C_{\mathbf{G}}^{(j)} = 1/S_0 \int_{S_0} \mathrm{d}^2\,\mathbf{R} \exp[-i(\mathbf{K}+\mathbf{G}).\mathbf{R}]\,\tau_j(\mathbf{R}), \tag{4.6}$$

which reduces to

$$C_{\mathbf{G}}^{(j)} = \sum_l a_l^{(j)} \exp(il\theta_{\mathbf{K}+\mathbf{G}})\, i^{-l}\, 2\pi/s_0 \times \int_0^{R_s} R\,\mathrm{d}R J_l(|\mathbf{K}+\mathbf{G}|R)\,\tau_l(R) \tag{4.7}$$

when S_0 is again replaced by a Wigner–Seitz circle and the angular integration carried out.

In Fig. 7, for Bloch waves (2) and (4) of Au [111] at 613 keV, we plot the contribution from each partial wave to the sum in (4.4). As expected, these Bloch waves are *sp* hybrids near $\bar{\Gamma}$, the hybridization persisting almost up to $\mathbf{K} = 0$ because of the accidental degeneracy of bands (2), (3) and (4) at this voltage. Only for very small values of $|\mathbf{K}|$ does Bloch wave (2) become a pure *s* state and wave (4) a pure *p* state, indicating that the critical voltage when the states remain degenerate at $\mathbf{K} = 0$ is just above 613 keV. Bloch wave (3) however, remains a pure *p* state near $\bar{\Gamma}$ and is unaffected by the very rapid changes in waves (2) and (4). In a second paper, we shall show how the behaviour of Bloch waves (2) and (4) is responsible for the central bright spot observed in bright-field micrographs at the critical voltage (Shannon & Steeds, 1977).

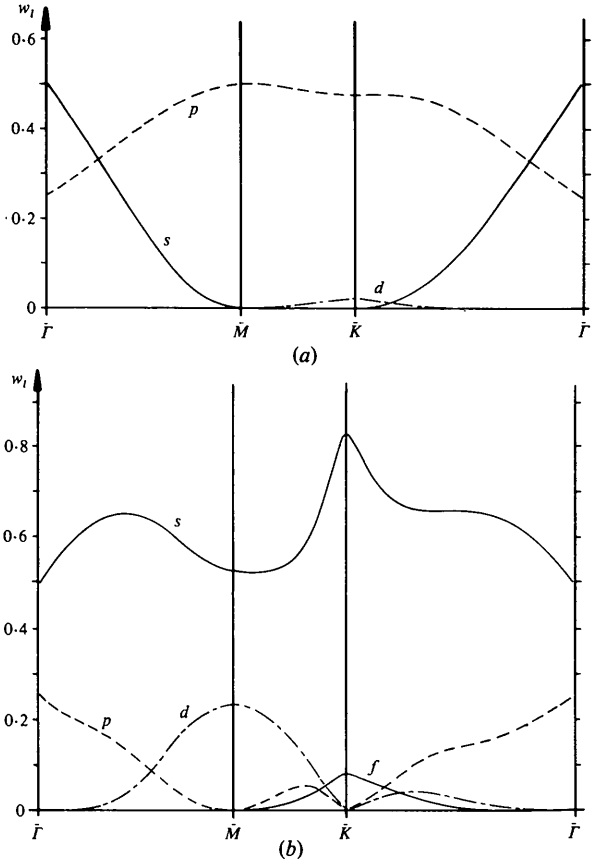

Fig. 7. Weights of the *s*, *p*, *d* partial waves as described in the text, (*a*) for Bloch wave (2) and (*b*) for Bloch wave (4).

However, before the ASA can be used to calculate diffracted wave intensities we must assess the accuracy of the ASA Bloch waves. In Fig. 8, therefore, we compare values of $|C_0^{(j)}|$ for Bloch waves (1), (2) and (4) as computed from (4.7) with a many-beam calculation and in Fig. 9 make a similar comparison for $|C_{202}^{(j)}|$ and $|C_{022}^{(j)}|$. For Bloch waves (2) and (4), the curves do not continue up to the centre of the Brillouin zone because of the rapid change in the *sp* hybridization of these waves near the accidental degeneracy. It can be seen that the agreement is considerably better in Fig. 8. This is because the $C_0^{(j)}$ are, according to (4.7), a cylindrical average of the Bloch waves and therefore less sensitive to the replacement of the unit cell of the projected potential by its Wigner–Seitz circle than the $C_{\mathbf{G}}^{(j)}$. For large values of $|\mathbf{G}|$ when the Fourier integral (4.6) is sensitive to the form of the wave function in the interstitial region, there can be large errors in the values of the Fourier coefficients $C_{\mathbf{G}}^{(j)}$ calculated from (4.7). However, to explain the observed zone-axis critical-voltage effects (Shannnon & Steeds, 1977), we only need the $C_0^{(j)}$ which may be obtained from (4.7). Furthermore, since only a 3 × 3 ASA matrix need be used near the centre of the Brillouin zone for small $\mathbf{K}$, in a subsequent paper we shall show how the bright-field intensity $I_0(\mathbf{K})$ can be calculated analytically near the critical voltage.

5. Summary and conclusions

From the KKR method proposed by Ozorio de Almeida (1975*a*), we have derived an approximate way of calculating the Bloch waves, τ_j, and their transverse energies, $s_j(\mathbf{K})$ (and hence the dispersion surface), in cross-grating HEED, *without* having to manipulate large matrices. Numerical tests of this atomic-string approximation (or ASA) for a Au [111] zone axis at 100, 613 and 1000 keV have shown that it yields extremely accurate values for the transverse energy bands when compared with large many-beam calculations. Similar results (not presented here) for Ge [111] and Cr [111] zone axes confirm that this level of agreement can be expected in general as long as the many-beam calculation has converged. Indeed, for Mo [111] at 293 K and 830 keV, which has a very strong projected potential, comparison with an exact APW calculation showed that the ASA which only used a small 7 × 7 matrix was better than a 127 × 127 many-beam calculation.

It has also been shown by comparison with the eingenvectors $C_{\mathbf{G}}^{(j)}$ of many-beam computations for Au [111] that the Bloch waves themselves may be calculated fairly accurately in the ASA even though the unit cell of the projected potential is replaced by its

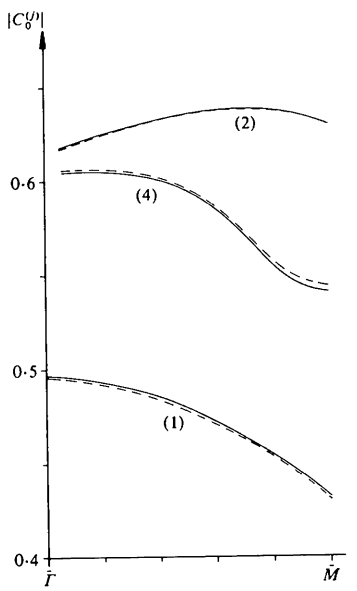

Fig. 8. Comparison of $|C_0^{(j)}|$ for Au [111] along $\bar{\Sigma}$ at 613 keV for Bloch waves (1), (2) and (4), (– – –) ASA, (——) many-beam.

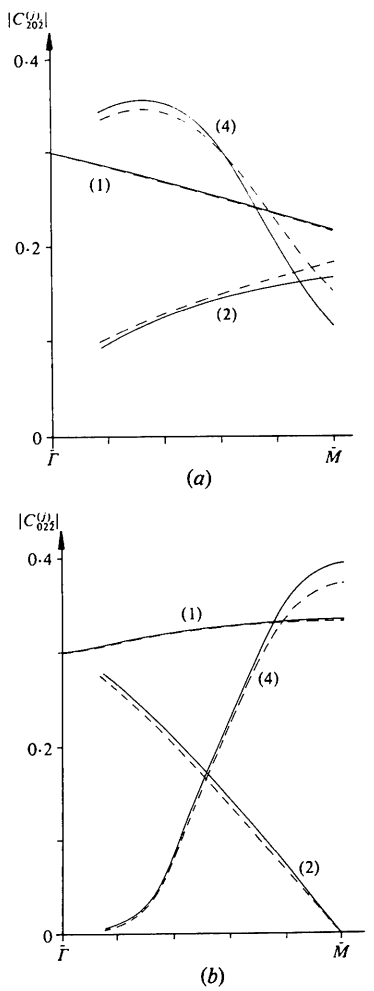

Fig. 9. Comparison of (*a*) $|C_{202}^{(j)}|$ and (*b*) $|C_{022}^{(j)}|$ as in Fig. 8.

Wigner–Seitz circle. In particular, this approximation caused little error (<0·5%) in the $C_0^{(j)}$ so the ASA can be used, for example, to calculate bright-field intensities.

The computations also showed that when the Sturm sequence described in the Appendix was used to locate the roots of the ASA determinant and the log derivatives were interpolated, an ASA calculation of the transverse energy bands was approximately ten times faster than the conventional many-beam method. However, when the Fourier coefficients, $C_G^{(j)}$, were also calculated, the large number of integrations which had to be carried out in the ASA meant that the computation times were then roughly equal.

In § 3 we described in detail the behaviour of the structure constants, $\mathscr{S}_{ll'}(\mathbf{K})$, and the log derivatives. It was shown that Bloch waves (2), (3) and (4) which become accidentally degenerate at the zone-axis critical voltage were almost entirely *sp* hybrids. Moreover, for $|\mathbf{K}| \lesssim \frac{1}{4}(2\bar{2}0)$ near the centre of the Brillouin zone, the Bloch waves on these bands remain predominantly *sp* hybrids so a 3 × 3 ASA matrix may be used, greatly facilitating the derivation of the analytic results to be presented in a second paper.

It is a pleasure to acknowledge the many fruitful discussions with Dr J. W. Steeds which took place during this work, and to thank Dr W. Temmermann for advice about Andersen's atomic-sphere approximation and Mr C. M. M. Nex for advice and help with some of the computing. The financial support of the SRC is also gratefully acknowledged for a research studentship (PTT) and a research grant at the beginning of this project (BFB).

APPENDIX

Roots of the ASA determinant

One way to find the transverse energy bands, $s_j(\mathbf{K})$, would be to evaluate the ASA determinant, (2.29), at different trial values of s and look for its zeros by detecting a change of sign (say). Such a method, however, is very inefficient and unreliable even if Gaussian elimination (Wilkinson, 1965) is used to convert the ASA matrix to upper triangular form in order to evaluate the determinant, as very small steps in s must be used to avoid missing two roots. Even then it fails near a doubly-degenerate pair of roots. Moreover, there are poles in the determinant which can also change its sign. As can be seen from the ASA equations there are second-order poles whenever

$$D_l = |l| \quad \text{for } l \neq 0 \qquad (A.1)$$

and first-order poles when D_0 vanishes. Only the latter cause the sign of the determinant to change.

Fortunately, by writing the ASA equations in matrix form,

$$\mathsf{M}(s_j, \mathbf{K})\, c(s_j, \mathbf{K}) = 0, \qquad (A.2)$$

and considering the related *linear* eigenvalue problem (henceforth **K** is suppressed),

$$\mathsf{M}(s)\, c^{(i)}(s) = \lambda_i(s)\, c^{(i)}(s), \qquad (A.3)$$

at an arbitrary transverse energy, s, a simple method for finding *all* the eigenvalues s_j in some range (s_L, s_U) may be devised. The derivation follows that used by van der Avoird, Liebmann & Fassaert (1974) in their band-structure calculations. Differentiating (*A*.3) and assuming that the eigenvectors $c^{(i)}$ are normalized so that $c^{(i)\dagger} c^{(i)} = 1$, we find, since M is Hermitian, that

$$\frac{\partial \lambda_i}{\partial s} = c^{(i)\dagger} \frac{\partial \mathsf{M}}{\partial s} c^{(i)} = \sum_l \frac{1}{(|l| - D_l)^2} \frac{\partial D_l}{\partial s} |c_l^{(i)}|^2 \qquad (A.4)$$

from (2.25) and (2.26). But, from the Wronskian theorem (4.5), we know that $\partial D_l/\partial s$ is always negative [the $\tau_l(R)$ are real when absorption is neglected and $U_{MT}(R)$ is real], so (*A*.4) implies

$$\frac{\partial \lambda_i}{\partial s} < 0 \qquad (A.5)$$

for every linear eigenvalue for all s.

Immediately, we note this means that at least one λ_i has a *simple* zero at each transverse energy band, s_j. If s_j is non-degenerate *exactly* one λ_i is zero; if s_j is a doublet, *two* λ_i are zero, *etc.* Similarly, as shown by van der Avoird, Liebmann & Fassaert (1974), when there is a *simple* pole in det |M|, *one* of the λ_i has a simple pole, and *two* λ_i have simple poles at the second-order poles of det |M|. Thus, assuming a second-order pole in det |M| due to one of the $D_l = |l|$ for $l \neq 0$ as in (*A*.1), we may sketch the behaviour of the λ_i as in Fig. 10.

Besides showing how many transverse energy bands, $s_i(\mathbf{K})$, can be obtained from a small ASA matrix (there is an infinite sequence of poles in each log derivative and therefore an infinite sequence of poles in the λ_i), Fig. 10 may be generalized to yield a simple rule for counting the number of transverse energy bands $n(s_L, s_U)$ in the range s_L to s_U. Since $n(s_L, s_U)$ is equal to the number of zero λ_i in (s_L, s_U),

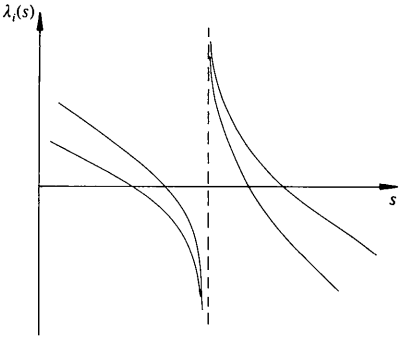

Fig. 10. The eigenvalues $\lambda(s)$.

$$n(s_L,s_U) = n_+(s_L) - n_+(s_U) + \sum_{s(m)} d_m, \qquad (A.6)$$

where $n_+(s)$ is the number of positive $\lambda_i(s)$ and the $\sum_{s(m)}$, which counts the number of poles in the λ_i, is over all zeros, $s(m)$, of $D_m - |m|$ in (s_L,s_U), with multiplicities, d_m, equal to one if m is zero and two otherwise. This is the same as the rule obtained by van de Avoird, Liebmann & Fassaert (1974) so we may take over the remainder of their scheme in which it is proved that

$$n_+(s) = \text{number of positive diagonal elements in the upper triangular form of M,} \qquad (A.7)$$

by using a Sturm sequence. Thus, since the upper triangular form of M may be quickly obtained by Gaussian elimination *without* pivoting (van der Avoird, Liebmann & Fassaert, 1974), once the $s(m)$ have been located in a preliminary calculation, all we have to do to find all the s_j in (s_L,s_U) is to construct $n(s_L,s_U)$ and then divide the range successively in half until each root is obtained with the desired accuracy.

In practice, to facilitate rapid evaluation of the log derivatives D_l at the required s, the wavefunctions, $\tau_l(R_s,s)$, and their derivatives, $\tau_l'(R,s)$, were approximated by polynomials (in s) fitted to a grid of points computed at the beginning of the calculation. These polynomials were then differentiated directly when we wished to evaluate the normalization integrals (4.4).

References

ABRAMOWITZ, M. & STEGUN, I. A. (1965). *Handbook of Mathematical Functions*. New York: Dover.

ANDERSEN, O. K. (1975). *Phys. Rev. B*, **12**, 3060–3083.

AVOIRD, A. VAN DER, LIEBMANN, S. P. & FASSAERT, D. J. M. (1974). *Phys. Rev. B*, **10**, 1230–1240.

BERRY, M. V. (1971). *J. Phys. C*, **4**, 697–722.

BERRY, M. V. & OZORIO DE ALMEIDA, A. M. (1973). *J. Phys. A*, **6**, 1451–1460.

BRADLEY, C. J. & CRACKNELL, A. P. (1972). *The Mathematical Theory of Symmetry in Solids*. Oxford: Clarendon Press.

BUXTON, B. F. (1976). *Proc. R. Soc. London Ser. A*, **350**, 335–361.

BUXTON, B. F. & LOVELUCK, J. E. (1977). *J. Phys. C*, **10**, 3941–3958.

BUXTON, B. F., LOVELUCK, J. E. & STEEDS, J. W. (1978*a*). *Electron Diffraction* 1927–1977, edited by P. J. DOBSON, J. B. PENDRY & C. J. HUMPHREYS, pp. 29–33. London and Bristol: Institute of Physics.

BUXTON, B. F., LOVELUCK, J. E. & STEEDS, J. W. (1978*b*). *Philos. Mag.* **A38**, 259–278.

BUXTON, B. F. & TREMEWAN, P. T. (1978). *Electron Diffraction* 1927–1977, edited by P. J. DOBSON, J. B. PENDRY & C. J. HUMPHREYS, pp. 13–17. London and Bristol: Institute of Physics.

CORNWELL, J. F. (1969). *Group Theory and Electronic Energy Bands in Solids*. Amsterdam: North-Holland.

DAVID, M., GEVERS, R. & SERNEELS, R. (1976). *Phys. Status Solidi B*, **74**, 359–373.

FUJIMOTO, F. (1978). *Phys. Status Solidi A*, **45**, 99–106.

FUJIMOTO, F., SUMIDA, N. & FUJITA, H. (1977). *J. Phys. Soc. Jpn*, **42**, 1274–1281.

FUJIMOTO, F., TAKAGI, S., KOMAKI, K., KOIKE, H. & UCHIDA, Y. (1972). *Radiat. Eff.* **12**, 153–161.

FUJIMOTO, F., UCHIDA, Y. & LEHMPFUHL, G. (1976). *Microscopie Electronique à Haute Tension* 1975, edited by B. JOUFFREY & P. FAVARD, pp. 109–112. Paris: Société Française de Microscopie Electronique.

FUJIWARA, K. (1961). *J. Phys. Soc. Jpn*, **16**, 2226–2238.

FUJIWARA, K. (1962). *J. Phys. Soc. Jpn*, **17**, Suppl. B-II, 118–123.

HIRSCH, P. B., HOWIE, A., NICHOLSON, R. B., PASHLEY, D. W. & WHELAN, M. J. (1965). *Electron Microscopy of Thin Crystals*. London: Butterworth.

HOWIE, A. (1966). *Philos. Mag.* **14**, 223–287.

JONES, P. M. (1976). *Microscopie Electronique à Haute Tension* 1975, edited by B. JOUFFREY & P. FAVARD, pp. 97–100. Paris: Société Française de Microscopie Electronique.

JONES, P. M. (1977). PhD Thesis, Univ. of Bristol.

KAMBE, K. (1978). *Electron Diffraction* 1927–1977, edited by P. J. DOBSON, J. B. PENDRY & C. J. HUMPHREYS, pp. 23–28. London and Bristol: Institute of Physics.

KAMBE, K. & LEHMPFUHL, G. (1974). *Diffraction Studies of Real Atoms and Real Crystals*, pp. III B-3/277–278. Melbourne: Australian Academy of Science.

KAMBE, K., LEHMPFUHL, G. & FUJIMOTO, F. (1974). *Z. Naturforsch. Teil A*, **29**, 1034–1044.

LIGHTHILL, M. J. (1958). *Introduction to Fourier Analysis and Generalized Functions*. London: Cambridge Univ. Press.

MESSIAH, A. (1961). *Quantum Mechanics*, Vol. 1. Amsterdam: North-Holland.

NIJBOER, B. R. A. & DE WETTE, F. W. (1957). *Physica*, **23**, 309–321.

OZORIO DE ALMEIDA, A. M. (1975*a*). *Acta Cryst.* A**31**, 435–442.

OZORIO DE ALMEIDA, A. M. (1975*b*). *Acta Cryst.* A**31**, 442–445.

SHANNON, M. D. & STEEDS, J. W. (1977). *Philos. Mag.* **36**, 279–307.

STEEDS, J. W., JONES, P. M., LOVELUCK, J. E. & COOKE, K. (1977). *Philos. Mag.* **36**, 309–322.

STEEDS, J. W., JONES, P. M., RACKHAM, G. M. & SHANNON, M. D. (1976). *Developments in Electron Microscopy and Analysis*, edited by J. A. VENABLES, pp. 351–356. London: Academic Press.

UCHIDA, Y., FUJIMOTO, F., KATERBAU, K.-H. & WILKENS, M. (1978). *Electron Diffraction* 1927–1977, edited by P. J. DOBSON, J. B. PENDRY & C. J. HUMPHREYS, pp. 18–22. London and Bristol: Institute of Physics.

WILKINSON, J. H. (1965). *The Algebraic Eigenvalue Problem*. Oxford: Clarendon Press.

ZIMAN, J. M. (1971). *Solid State Phys.* **26**, 1–101.